ISSN 1070-4272, Russian Journal of Applied Chemistry, 2009, Vol. 82, No. 8, pp. 1351−1356. © Pleiades Publishing, Ltd., 2009.
Original Russian Text © G.A. Voronova, M.P. Fedotova, E.Yu. Emel'yanova, O.V. Vodyankina, 2009, published in Zhurnal Prikladnoi Khimii, 2009, Vol. 82, No. 8, pp. 1256−1260.

INORGANIC SYNTHESIS AND INDUSTRIAL INORGANIC CHEMISTRY

Photocatalytic Properties of Electric-Explosion-Produced TiO_2 Nanopowder

G. A. Voronova[a], M. P. Fedotova[a], E. Yu. Emel'yanova[b], and O. V. Vodyankina[b]

[a] *Tomsk Polytechnic University, Tomsk, Russia*
[b] *Tomsk State University, Tomsk, Russia*

Received December 22, 2008

Abstract—Structural features and physicochemical and photocatalytic properties of an electric-explosion-produced titanium dioxide powder were studied by means of X-ray phase and X-ray diffraction analyses, transmission electron microscopy, thermal analysis, and optical spectroscopy.

DOI: 10.1134/S1070427209080060

At present, the practical application of photocatalysis is mostly restricted by the low sensitivity of photocatalysts to visible light and by the slow rate of photocatalytic reactions. Among photocatalysts, the wide-bandgap *n*-type semiconductor TiO_2 is the most promising for a wide variety of photocatalytic reactions because of its high activity, nontoxicity, and resistance to electrochemical and photochemical corrosion [1–3]. Among the main modifications of TiO_2 (rutile, anatase), the highest photochemical activity is exhibited by anatase whose energy gap is about 3.2 eV [3, 4]. It is believed that the higher activity of anatase, compared with rutile, is due to the higher lying Fermi level, better capacity for oxygen adsorption, and high degree of hydroxylation [3]. The maximum absorption by TiO_2 is in the near-UV spectral range ($\lambda < 400$ nm), and, therefore, UV irradiation at wavelengths shorter than 400 nm is necessary for a photocatalytic conversion involving TiO_2. Most of studies have been devoted to photocatalytic processes with a Degussa P25 TiO_2 commercial catalyst [4–6] whose activity is frequently taken as reference.

A promising method for synthesis of a wide variety of nanopowders of inorganic materials (metals, alloys, chemical compounds) is the method of an electric explosion of a conductor (EEC technique) [7]. Compared with other methods used to produce metal oxides by evaporation of a metal and its subsequent condensation and oxidation, etc. [8], synthesis of nanopowders by electric explosion is advantageous because of the direct conversion of electric power to heat. A pulsed volume heating provides high energy densities and fast rates of scattering and cooling of a substance. Particles produced in this way have size, structural, phase, defective, and other energy-saturated states [7].

The method in which a titanium dioxide powder is produced by an electric explosion of a titanium wire in an oxygen-containing atmosphere [7–10] makes it possible to obtain particles 10 to 300 nm in size and to control the chemical and phase composition and the structure of the nanopowder. Use of systems produced by an electric explosion as photocatalysts is rather promising because the nanopowder contains a large number of defects and, as a consequence, of active surface centers, as well. These studies are new and can expand application fields of nanopowders.

The aim of this study was to perform an integrated analysis of structural features and physicochemical and photocatalytic properties of an electric-explosion-produced titanium dioxide nanopowder.

EXPERIMENTAL

The titanium dioxide nanopowder (EEP TiO_2) was produced by an electric explosion of a titanium conductor in an oxygen-containing atmosphere (15 vol %).[a] The X-

[a] Laboratory at Advanced Powder Technologies Limited-Liability Company, Regional Innovation-Technological Center, Siberian Branch, Russian Academy of Sciences.

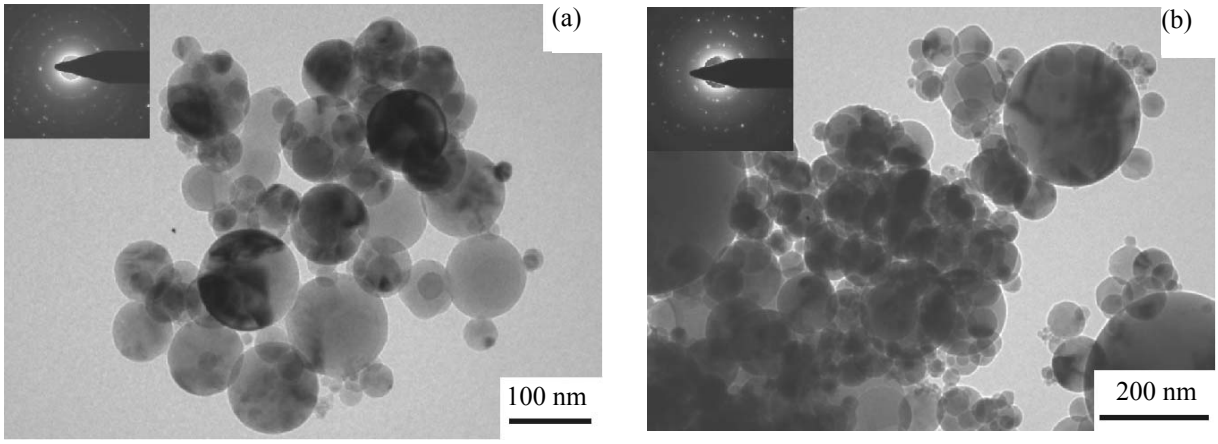

Fig. 1. TEM images of EEP TiO_2.

ray phase analysis was made on a Shimadzu XRD-6000 X-ray diffractometer with $Cu_{K\alpha}$ radiation. A quantitative analysis of the phase composition was performed using the PCPDFWIN database and a POWDER CELL 2.4 full-profile analysis software. The specific surface area was measured by the BET method from low-temperature adsorption of argon. The optical properties of EEP TiO_2 were studied by UV-Vis spectroscopy on a SHIMADZU UV-160A spectrophotometer. The size of powder particles was estimated by transmission electron microscopy (TEM) on a Philips CM 30 microscope. A thermal analysis was made using a NETZSCH STA 409 PG/PC derivatograph, with heating in an oxygen-containing medium to 1000°C at a rate of 10 deg min^{-1}.

For photoelectrochemical and photocatalytic studies, samples were immobilized on an electrically conducting substrate [6]. A glass plate with a fluorine-doped conducting SnO_2 layer served for this purpose. A sample was deposited onto the plate by electrophoresis from a stabilized suspension of the powder in ethanol (0.2 g/250 ml). The thickness h (μm) of the coatings was varied by changing the electrophoresis duration (s) and calculated from the change in the substrate mass, Δm (g). The coatings (electrodes) obtained were frontally exposed to light from a UV source (Zeiss ST 41 calibrated high-pressure mercury lamp with a 365-nm filter), with the generated photocurrent recorded. The actinometry of the light source was carried out using a Hamamatsu S1337-1010BQ Si photodiode. The intensity P of light was 2.0×10^8 photons s^{-1}. The photocurrent I_{ph} at the working electrode (difference of light and dark currents, I_l and I_d) was recorded polarographically (PU-1 polarograph) in a three-electrode scheme [11]: Ag/AgCl reference electrode (3 M KCl solution), platinum auxiliary electrode, and glass/F:SnO_2/EEP TiO_2 working electrode. A 1 mM solution of oxalic acid $H_2C_2O_4$ in 1 mM of K_2SO_4 served as a supporting electrolyte.

The photocatalytic activity of EEP TiO_2 was examined using the flow-through method in the course of $H_2C_2O_4$ decomposition [12]. Changes in the $H_2C_2O_4$ concentration (c_0 = 1 mM) were determined from a decrease in the concentration of total organic carbon (TOC) with a Shimadzu 5000 automated TOC analyzer with an autobatching unit. Experiments were performed in a flow-through steel reactor with a planar optical window, with a 0.6-μm-thick layer of the photocatalyst deposited onto its inner wall. The window was frontally exposed to light from a UV source. The $H_2C_2O_4$ solution was delivered by a micropump with a controllable flow rate.

EEP TiO_2 produced by the electric explosion of a titanium wire is a light gray powder. TEM micrographs of EEP TiO_2 are shown in Fig. 1. It can be seen that powder

Table 1. Structural Characteristics of EEP TiO_2 and Degussa P25 TiO_2

Sample	Phases found	Content of phases, vol %	CSR size, nm	$\Delta d:d \times 10^{-3}$
EEP TiO_2	Anatase	77	52.0	4.65
	Rutile	23	20.17	1.75
Degussa P25 TiO_2	Anatase	84	27.65	6.20
	Rutile	16	41.75	5.30

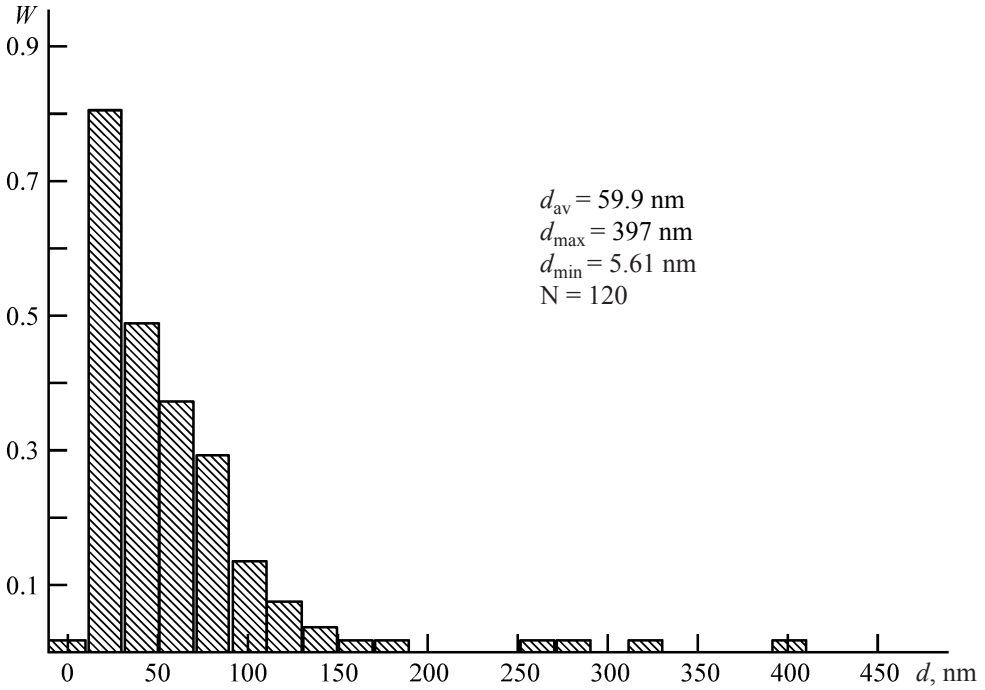

Fig. 2. Particle size distribution of EEP TiO_2, according to TEM data. (*W*) Fraction of particles of a given size and (*d*) particle diameter.

particles (30 to 350 nm in size) mostly have a regular spherical shape and are strongly agglomerated (Figs.1a, 1b).

The TEM data were used to construct a particle size distribution histogram for EEP TiO_2 (Fig. 2). It can be seen that the distribution is monomodal and has a sharp frontal peak and an extended rear part. The distribution has a maximum at particle diameters of 20–30 nm. The average particle size is 60 nm. Coarser particles (350 to 400 nm in diameter) also occur, which is due to specific features of the synthesis technology [7, 9, 10]. Thus, according to the available classification, the material can be identified as belonging to a nanostructured type.

The efficiency of photoinduced generation of carriers responsible for the photocatalytic activity and their subsequent diffusion in the bulk and on the surface of particles may be higher for an EEP TiO_2 sample constituted by agglomerates of different-size particles.

The specific surface area S_{sp} of the sample under study was 17 $m^2\ g^{-1}$, and that of the reference Degussa P25 TiO_2 sample, 55 $m^2\ kg^{-1}$. The relatively small specific surface area of EEP TiO_2, compared with the reference, is due to the considerable fraction of particles whose diameter exceeds the average particle size determined by TEM. Microdiffraction patterns of EEP TiO_2 (insets in Fig.1) have the form of well-resolved rings constituted by

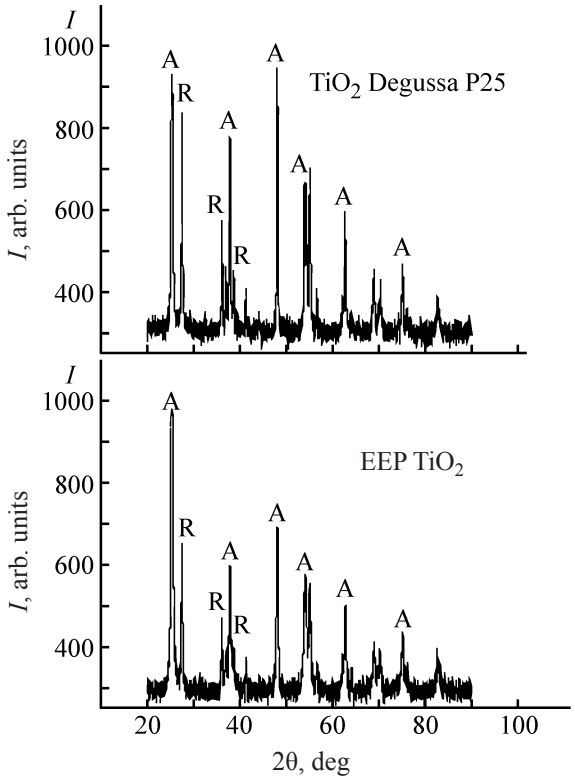

Fig. 3. X-ray diffraction patterns of EEP TiO_2 and Degussa P25 TiO_2. Phase designations: A, anatase; R, rutile. (*I*) Intensity and (2θ) Bragg angle.

Table 2. Activity of EEP TiO_2 and Degussa P25 TiO_2 in photocatalytic oxidation of $H_2C_2O_4$ (c_0 = 1 mM)

V, ml h^{-1}	EEP TiO_2			Degussa P25 TiO_2		
	c(TOC), mM	Δc(TOC), %	V (10^{12} mol s^{-1} cm^{-2})	c(TOC), mM	Δc(TOC), %	V (10^{12} mol s^{-1} cm^{-2})
6.5	0.24	87.9	1.17	0.18	91.0	0.23
22.8	0.54	72.9	3.42	0.17	91.5	0.71
40.8	1.03	48.3	4.06	0.18	91.0	1.35
80.4	1.51	24.4	4.04	0.34	83.0	2.24
162.8	1.75	12.7	4.26	0.72	64.0	3.16

separate resolved reflections. A microdiffraction pattern of this kind is characteristic of nanocrystalline systems.

Figure 3 shows X-ray diffraction patterns of EEP TiO_2 and Degussa P25 TiO_2. Table 1 lists XPA data. The X-ray phase analysis demonstrated the presence of two main phases in the samples studied: anatase and rutile. According to X-ray data, these phases are well crystallized (Table 1). The contents of the phases in EEP TiO_2 and Degussa P25 TiO_2 differ only slightly. The size of the coherent scattering region (CSR), found by the Scherrer method for EEP TiO_2, is approximately two times larger and two times smaller for anatase and rutile, respectively, compared with similar values for Degussa P25 TiO_2.

According to thermal analysis data, EEP TiO_2 is not oxidized on being heated in an oxygen-containing medium, which indicates that there is no metallic titanium incompletely oxidized in the electric explosion.

The absorption spectrum of a sample is shown in Fig. 4. The absorption peak of the EEP TiO_2 samples lies in the near-UV region, in agreement with the value E_g = 3.2 eV for TiO_2. Thus, the photoactivity of EEP TiO_2 will be manifested under the action of light with a wavelength shorter than 388 nm [3]. With these parameters, the absorption efficiency of solar light reaching the Earth's surface is as low as 3–4%.

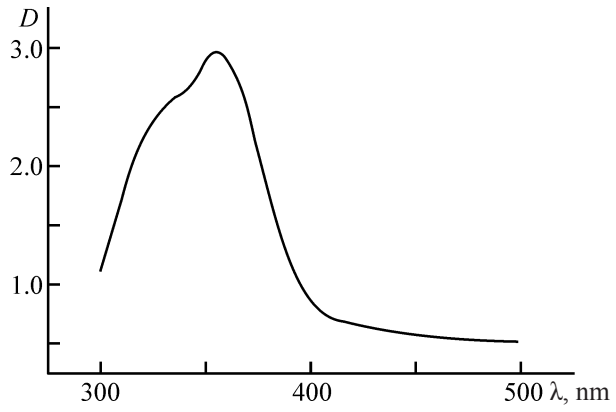

Fig. 4. Absorption spectrum of an EEP TiO_2 sample. (D) Absorption efficiency and (λ) wavelength.

To enable analysis of the nature of the photocatalytic activity of EEP TiO_2, Fig. 5 shows how the current in the three-electrode system (working electrode/EEP TiO_2/electrically conducting substrate; 0.6-μm-thick EEP TiO_2 coating) depends on the applied potential. The photocurrent I_{ph} (μA) was recorded as a difference of the light (I_l) and dark (I_d) currents in a periodic exposure of the EEP TiO_2 to light from the UV source.

According to the data obtained, changing the applied potential from –0.6 to 0.8 V leads to an increase in both the light and dark currents of the working electrode, with the current increasing more noticeably upon illumination of the working electrode, which is due to the appearance of a photocurrent I_{ph} in the system. On sweeping the

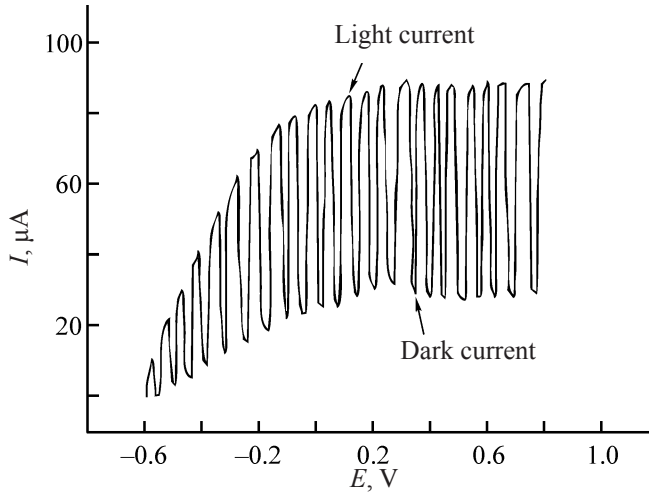

Fig. 5. Photocurrent at the glass/F:SnO2/EEP TiO_2 sample in a solution of 1 mM of $H_2C_2O_4$ and 1 mM of K_2SO_4 under periodic UV irradiation. (I) Current and (E) potential.

potential, I_{ph} increases and, at potentials of 0.2–0.3 V, reaches the maximum value of 40–45 μA. Further increase in the potential does not lead to any noticeable change in I_l and I_d or in I_{ph}. The run of the current–voltage (*I–V*) dependence shows that, at applied potentials of 0.3 V and higher (relative to the silver chloride electrode), the efficiency of the photoinduced process of formation of an electron–hole pair on EEP TiO_2 is the highest. The applied potential hinders carrier recombination. The *I–V* characteristics of the electrodes were used to estimate the photoinduced carrier generation process.

The quantum efficiencies of the process on EEP TiO_2 and Degussa P25 TiO_2 were estimated by the method described in [11, 12]. The degree Φ of conversion of absorbed photons to the current at the working electrode was calculated by the formula

$$\Phi = \frac{1}{FPS},$$

where *I* is current (A); *F*, Faraday constant (96 485 C mol^{-1}); *P*, light intensity (*W* cm^{-2}); and *S*, illuminated electrode area (cm^2).

The calculation demonstrated that, for the sample under study, Φ = 0.04, whereas for the reference, Φ = 0.02 at the same light absorption $(1 - T) \approx 0.8$ (from UV-Vis absorption data). Thus, for the EEP TiO_2, the quantum efficiency of the photoinduced process is twice that for Degussa P25 TiO_2 commercial catalyst. This difference may be due to different crystal structures of samples (Table 1). The ratio between the crystallite sizes of the anatase and rutile phases in EEP TiO_2 exceeds that in Degussa P25 TiO_2.

The photocatalytic properties of the samples were studied in a model reaction of $H_2C_2O_4$ decomposition. The photocatalytic oxidation of oxalic acid is a single-stage two-electron redox reaction whose products are carbon dioxide and water [6]. To improve the process efficiency, a potential of 0.6 V (relative to steel) was applied with a potentiostat to the working surface of the reactor (conducting glass with a deposited EEP TiO_2 layer) in order to raise the carrier separation efficiency. The photocatalytic properties of EEP TiO_2 and a commercial sample of Degussa P25 TiO_2 are listed in Table 2.

If the solution delivery rate is raised, the degree of $H_2C_2O_4$ conversion (in terms of TOC) in a solution at the reactor outlet decreases for both samples, which is due to a shorter time of contact. Under the conditions studied, the degree of $H_2C_2O_4$ conversion, calculated from the decrease Δ*c* in the TOC concentration, is higher for Degussa P25 TiO_2 sample, which is particularly noticeable at a short contact time. This difference is probably observed because the specific surface areas of the samples differ by nearly a factor of 3: 17 and 55 $m^2 g^{-1}$ for EEP TiO_2 and Degussa P25 TiO_2, respectively. When comparing photocatalytic activities, it is better to reduce the reaction rate to the specific surface area of a catalyst. The reduced reaction rate *V* (mol s^{-1} cm^{-2}) is higher for the sample under study, compared with the commercial Degussa P25 TiO_2, in the entire range of solution flow rates *V* (Table 2). The exceeding activity of EEP TiO_2 is due to the presence of different-size particles in its composition, existence of agglomerates of particles of this kind, and differences in crystal structure.

CONCLUSIONS

(1) The rate of the photocatalytic decomposition of $H_2C_2O_4$ with an electric-explosion-produced TiO_2 nanopowder is higher, compared with Degussa P25 TiO_2 commercial catalyst.

(2) The exceeding activity of the electric-explosion-produced TiO_2 nanopowder is accounted for by the presence of different-size particles and agglomerates of particles of this kind in its composition and by the crystal structure different from that of the commercial catalyst.

(3) The development of electroexplosive techniques for synthesis of a TiO_2 nanopowder and its use as a photocatalyst are promising.

ACKNOWLEDGMENTS

The study was supported by a CRDF grant (Y3-MP-16-03) and by the RF Presidential Council for grants (no. MD-968.2007.3).

REFERENCES

1. Mills, A. and Le Hunte, S., *J. Photochem. Photobiol. A: Chem.*, 1997, vol. 108, pp. 1–35.
2. Mills, A. and Lee, S.-K., *J. Photochem. Photobiol. A: Chem.*, 2002, vol. 152, p. 233.
3. Anpo, M. and Takeuchi, M., *J. Catal.*, 2003, vol. 216, pp. 505–516.
4. Carp, O., Huisman, C.L., and Reller, A., P*rogr. Solid State Chem.*, 2004, vol. 32, pp. 33–177.
5. Bauer, R., Waldner, G., Fallmann, H., et al., *Catal. Today,*

1999, vol. 53, no. 1, pp. 131–144.

6. Byrne, J.A. and Eggins, B.R., *J. Electroanal. Chem*., 1998, vol. 457, pp. 61–72.
7. Lerner, M.I., *Electric-Explosion-Produced Nanopowders of Inorganic Materials: Manufacture Technology, Characteristics, Application Fields,* Doctoral Dissertation, Tomsk, 2007.
8. Kupriyanov, L.Yu., Galyamov, B. Sh., Zav'yalov, S.A., and Negin, A.E., *Russian J. of Phys. Chem*., 2004, vol. 78, no. 4, pp. 515–521.
9. Lerner, M.I., Davydovich, V.I., and Svarovskaya, N.V., *Fiz. Mezomekhanika*, 2004, no. 7, part 2, pp. 340–343.
10. Lerner, M.I., *Izv. Vyssh. Uchebn. Zaved., Fiz*., 2006, vol. 49, no. 6, pp. 91–95.
11. Waldner, G., Pourmodjib, M., Bauer, R., and Neumann-Spallart, M., *Chemosphere*, 2003, vol. 50, pp. 989–998.
12. Krysa, J., Keppert, M., Waldner, G., and Jirkovsky, J., *Electrochim. Acta*, 2005, vol. 50, pp. 5255–5260.